Journal of Alloys and Compounds 517 (2012) 31–39

Contents lists available at SciVerse ScienceDirect

Journal of Alloys and Compounds

journal homepage: www.elsevier.com/locate/jallcom

Experimental investigation and thermodynamic prediction of the Cu–Sb–Zn phase diagram

Duško Minić[a,*], Dragan Manasijević[b], Vladan Ćosovic[c], Nadežda Talijan[c], Živan Živković[b], Dragana Živković[b], Milena Premović[a]

[a] University of Pristina, Faculty of Technical Sciences, 38220 Kosovska Mitrovica, Serbia
[b] University of Belgrade, Technical Faculty, 19210 Bor, Serbia
[c] University of Belgrade, Institute of Chemistry, Technology and Metallurgy, 11000 Belgrade, Serbia

ARTICLE INFO

Article history:
Received 7 October 2011
Received in revised form
23 November 2011
Accepted 26 November 2011
Available online 6 December 2011

Keywords:
Cu–Sb–Zn ternary alloy system
Thermal properties
Phase diagram
SEM-EDS

ABSTRACT

Ternary Cu–Sb–Zn system has been thermodynamically assessed by using CALPHAD method and experimentally by DSC and SEM-EDS methods. The liquidus projection, invariant equilibria, several vertical sections and isothermal sections at 450 °C and 25 °C were predicted using COST 531 Thermodynamic Database. Phase transition temperatures of alloys along three predicted vertical sections of the Cu–Sb–Zn ternary system with molar ratios Cu:Zn = 1:3, Cu:Zn = 1 and Sb:Zn = 1, were determined by DSC analysis. Predicted isothermal sections at 450 °C and 25 °C were compared with the results of the SEM-EDS analysis. The calculated values were found to be in a good agreement with the experimentally obtained values and literature data.

1. Introduction

Investigations into the alternative low temperature solders, in the light of environmental and health concerns, have been carried out by numerous authors for quite some time now. Taking into consideration the importance of the lead-free solders, in recent years these investigations are extended to the high temperature ternary systems with copper. These systems are of great interest due to wide application of these alloys in various industries.

For this reason, in the present study, the ternary Cu–Sb–Zn system has been thermodynamically assessed through experimental and theoretical investigation of phase transition temperatures, liquidus projection, invariant equilibria, three vertical sections and isothermal sections at 450 °C and 25 °C. Experimental results obtained using differential scanning calorimetry (DSC) and scanning electron microscopy (SEM) combined with energy dispersive spectrometry (EDS) are compared with the results of thermodynamic binary-based prediction, based on the 4.4 SGTE values of Gibbs energies for pure elements [1] and thermodynamic binary data included in the, COST 531, Version 1.0, Thermodynamic Database [2].

2. Experimental procedure

All samples were prepared by melting Cu, Sb and Zn pellets of 99.99 at.% purity in an induction furnace, under high purity argon atmosphere. Given that Sb is easy to volatilize, before melting, an extra amount of Sb (about 3–5 at.%) was added to compensate the weight loss. Microstructures of the selected samples and chemical compositions of the equilibrium phases were determined using JEOL JSM-6460 scanning electron microscope (SEM) equipped with Oxford Instruments energy dispersive spectrometer (EDS). The samples for SEM-EDS investigation were annealed at 450 °C for 200 h and subsequently quenched into ice water.

Thermal behavior of the selected alloy samples was investigated by DSC method using TA instruments SDT Q600 thermal analyzer. Phase transformation temperatures were determined at 5 °C/min heating rate under dynamic argon atmosphere. Used sample mass and applied heating rate were selected on the basis of the previous analysis of $Cu_{0.55}Sb_{0.225}Zn_{0.225}$ alloy samples under different testing conditions.

Composition of the investigated alloy samples from Cu:Zn = 1:3 and Sb:Zn = 1 vertical cross sections was varied by gradual increase of molar ratio of antimony and copper by 0.1. Due to the simplicity of the third vertical section (Cu:Zn = 1), molar ratio of antimony was gradually increased by 0.2.

3. Thermodynamic models and crystallographic data

Phase diagram of the Cu–Sb–Zn ternary system was calculated by CALPHAD method [3,4] using only optimized thermodynamic parameters for constitutive binary systems. The basic mathematical method used for calculation of phase equilibria is a constrained minimization of Gibbs energy for a given temperature, pressure and overall composition, which is common approach for all currently available software packages for modeling of thermodynamic

* Corresponding author. Tel.: +381 63 7025683.
E-mail address: dminic65@open.telekom.rs (D. Minić).

0925-8388/$ – see front matter © 2011 Elsevier B.V. All rights reserved.
doi:10.1016/j.jallcom.2011.11.130

properties and phase diagrams of multi-component systems. The molar Gibbs energy of a phase ϕ can be considered as the sum of a number of different contributions:

$$G_m^\phi = G_{ref}^\phi + G_{id}^\phi + G_E^\phi + G_{mag}^\phi + G_P^\phi + \cdots \quad (1)$$

where G_{ref}^ϕ is the molar Gibbs energy of the weighted sum of the system constituents i (elements, species, compounds, etc.) of the phase ϕ relative to the chosen reference state (typically the Stable Element Reference state – SER),

$$G_{ref}^\phi = \sum_{i=1}^{n} x_i \cdot {}^oG_i^\phi \quad (2)$$

and its temperature dependence is given by

$$G(T) = a + bT + cT\ln(T) + \sum_i d_i T^n \quad (3)$$

where $a - d_i$ are adjustable coefficients.

G_{id}^ϕ is a contribution to the Gibbs energy from ideal random mixing of the constituents on the crystal lattice for an n-constituent system, given as

$$G_{id}^\phi = RT\sum_{i=1}^{n} x_i \ln(x_i), \quad i = 1, \ldots, n \quad (4)$$

G_E^ϕ is the excess Gibbs energy, which describes the influence of non-ideal mixing behavior on the thermodynamic properties of a solution phase. It is given by the Muggianu extension of the

Table 1
Considered phases and their crystal structures [8].

Phase common names	Thermodynamic database name	Pearson's symbol
L	LIQUID	–
(Zn)	HCP_ZN	*hP2*
(Cu)	FCC_A1	*cF4*
(Sb)	RHOMBO_A7	*hR2*
$CuZn_5$	HCP_A3	*hP2*
β_CuZn	BCC_A2	*cI2*
$CuZn_3$	BCC_A2	*cI2*
Cu_5Zn_8	CUZN_BRASS	*cI52*
β′_CuZn	B2_BCC	*cP2*
δ_Sb_3Zn_4 ($Sb_{3.094}Zn_{3.906}$)	SBZN_DELTA	...
γ_Sb_3Zn_4 ($Sb_{3.087}Zn_{3.913}$)	SBZN_GAMMA	...
ξ_Sb_2Zn_3 ($Sb_{2.025}Zn_{2.975}$)	SBZN_ZETA	*oI**
SbZn	SBZN_BETA	*oP16*
Sb_3Zn_4	SBZN_EPSILON	...
Sb_2Zn_3	SBZN_ETA	*oP30*
Cu_2Sb	CUSB_ETA	*tP6*
$Cu_{73}Sb_{20}$	CUSB_ZETA	*hP26*
$Cu_{10}Sb_3$	CUSB_EPSILON	*oP8*
Cu_9Sb_2	CUSB_DELTA	*hP**
$Cu_{11}Sb_2$	CUSB_GAMMA	*hP2*
Cu_3Sb	BCC_A2	*oF16*

Redlich–Kister formalism [5,6]

$$G_E^\phi = \sum_{\substack{i,j=1 \\ i\neq j}}^{n} x_i x_j \sum_{Z=0}^{m} {}^Z L (x_i - x_j)^Z + \sum_{\substack{i,j,k=1 \\ i\neq j\neq k}}^{n} x_i x_j x_k L_{ijk}, \quad z = 0, \ldots m \quad (5)$$

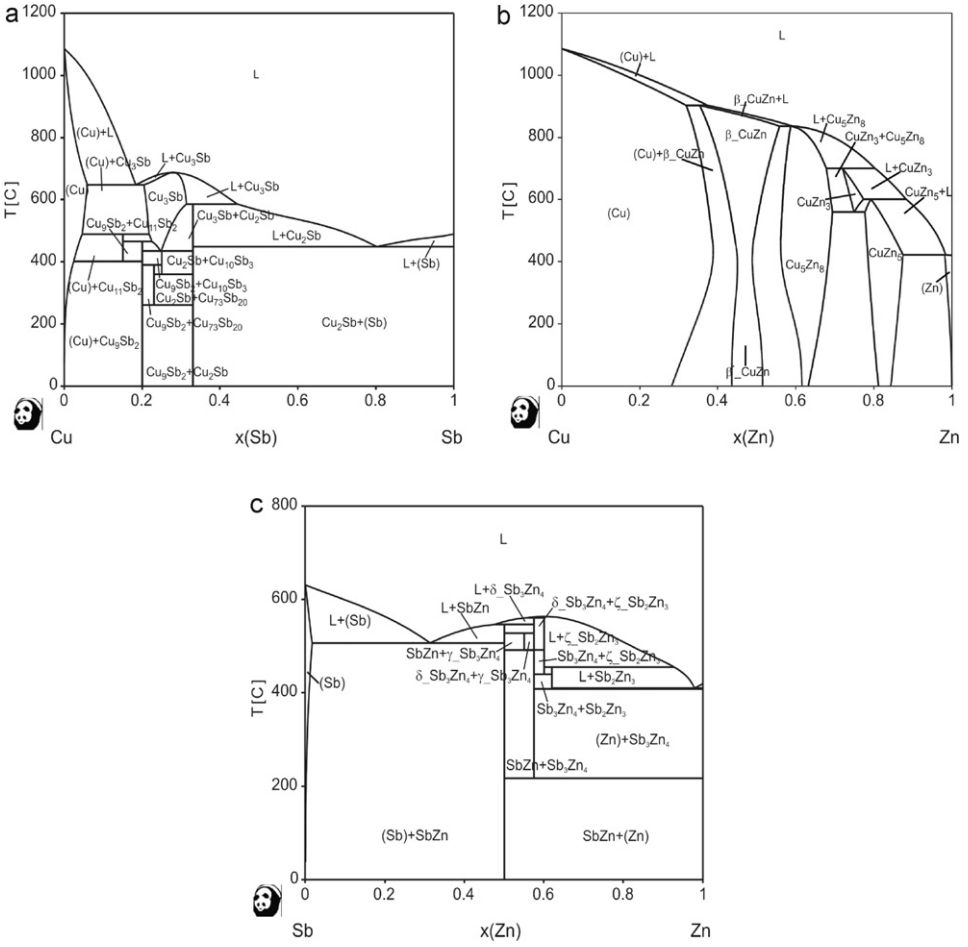

Fig. 1. Calculated phase diagrams of (a) Cu–Sb, (b) Cu–Zn and (c) Sb–Zn binary systems.

Table 2
Comparative review of DSC results and calculated results for the investigated alloys of the Cu–Sb–Zn ternary system.

Alloy composition	Phase transition temperatures (°C)					
	Liquidus temperature		Temperatures invariant reactions		Temp. monovariant reactions	
	Exp.	Calc.	Exp.	Calc.	Exp.	Calc.
***x*(Cu)**	***x*(Sb)/*x*(Zn) = 1**					
0.1	520	516.6	380	388.3	–	–
0.2	494	486.7	382	388.3	–	–
0.3	446	441.9	384	382.5	–	–
0.4	383	381	–	–	–	–
0.5	452	452.3	381	388.3	–	–
0.55	523	507.4	413; 465	397.7; 441.1	480	478.6
0.6	582	571.6	375; 442	379.3; 440	501	497.3
0.7	709	707.5	113; 267; 521	115.6; 257.7; 500.8	–	–
0.8	840	836.3	–	–	445; 611	435; 601
0.9	991	992	–	–	464; 624	460; 629
***x*(Sb)**	***x*(Cu)/*x*(Zn) = 1/3**					
0.1	672	657.7	293; 476	297.1; 478.7	–	–
0.2	551	575.3	494	485.4	–	–
0.3	498	493.4	382	382.8	–	–
0.4	512	509.2	385	378.9	–	–
0.5	502	498.3	381	388.7	–	–
0.6	495	490.5	395	388.7	–	–
0.7	534	537.6	393	388.7	–	–
0.8	572	575.3	402	388.7	501	493.6
0.9	602	601.7	401	388.7	498	485.4
***x*(Sb)**	***x*(Cu)/*x*(Zn) = 1**					
0.2	567	559	382	380.1	–	–
0.4	426	424.4	387	380.1	–	–
0.6	523	507.4	402	387.6	–	–
0.8	602	573.6	403	387.6	–	–

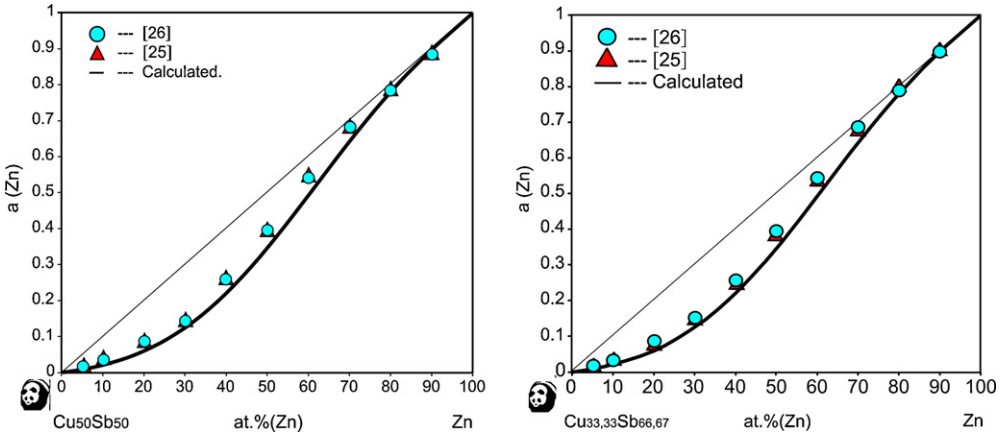

Fig. 2. Comparative presentation of the calculated and literature values of activities of Zn for two vertical sections: (a) $Cu_{50}Sb_{50}$–Zn and (b) $Cu_{33.33}Sb_{66.67}$–Zn.

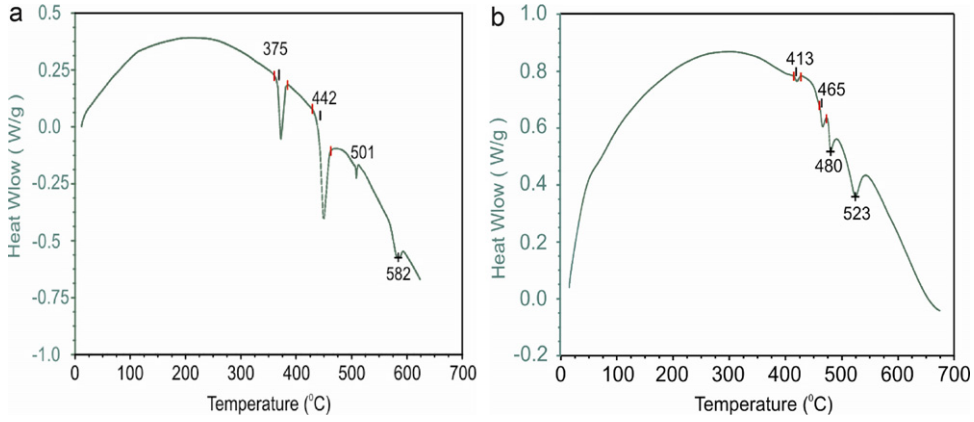

Fig. 3. DSC curves of: (a) $Cu_{0.6}Sb_{0.2}Zn_{0.2}$ and (b) $Cu_{0.55}Sb_{0.225}Zn_{0.225}$ alloys.

Table 3
Calculated and experimentally determined phase compositions in the ternary Cu–Sb–Zn system at 450 °C.

Sample	Overall composition (at.%)	Theoretically predicted phases	Experimentally determined phases	Compositions of phases (at.%)					
				Cu		Sb		Zn	
				Exp.	Calc.	Exp.	Calc.	Exp.	Calc.
	9 Cu	SbZn	SbZn	0.88	–	51.08	50	48.04	50
1(△)	60 Sb	(Sb)	(Sb)	0.68	–	95.56	98.76	3.76	1.24
	31 Zn	L	L	19.73	21.32	49.96	48.77	30.31	29.92
	31 Cu								
2(□)	49 Sb	(Sb)	(Sb)	1.92	–	95.44	99.39	2.64	0.61
	20 Zn	L	L	33.05	33.41	45.05	44.37	21.9	22.22
	38 Cu	Cu_2Sb	Cu_2Sb	64.58	67	34.77	33	0.65	–
3(○)	51 Sb	(Sb)	(Sb)	3.35	–	95.63	99.58	1.02	0.42
	11 Zn	L	L	38.58	38.04	44.07	43.45	17.35	18.51
	26 Cu	Cu_5Zn_8	Cu_5Zn_8	38.72	39.8	–	–	61.28	60.2
4(▽)	19 Sb	SbZn	SbZn	2.88	–	49.27	50	47.85	50
	54 Zn	L	L	28.63	28.52	33.74	31.61	37.63	39.87
	59 Cu	Cu_2Sb	Cu_2Sb	65.25	67	32.74	33	2.01	–
5(◊)	22 Sb	(Cu)	(Cu)	60.84	62.69	1.05	0.23	38.11	37.08
	19 Zn	L	L	53.95	50.22	23.17	24.86	22.88	24.92

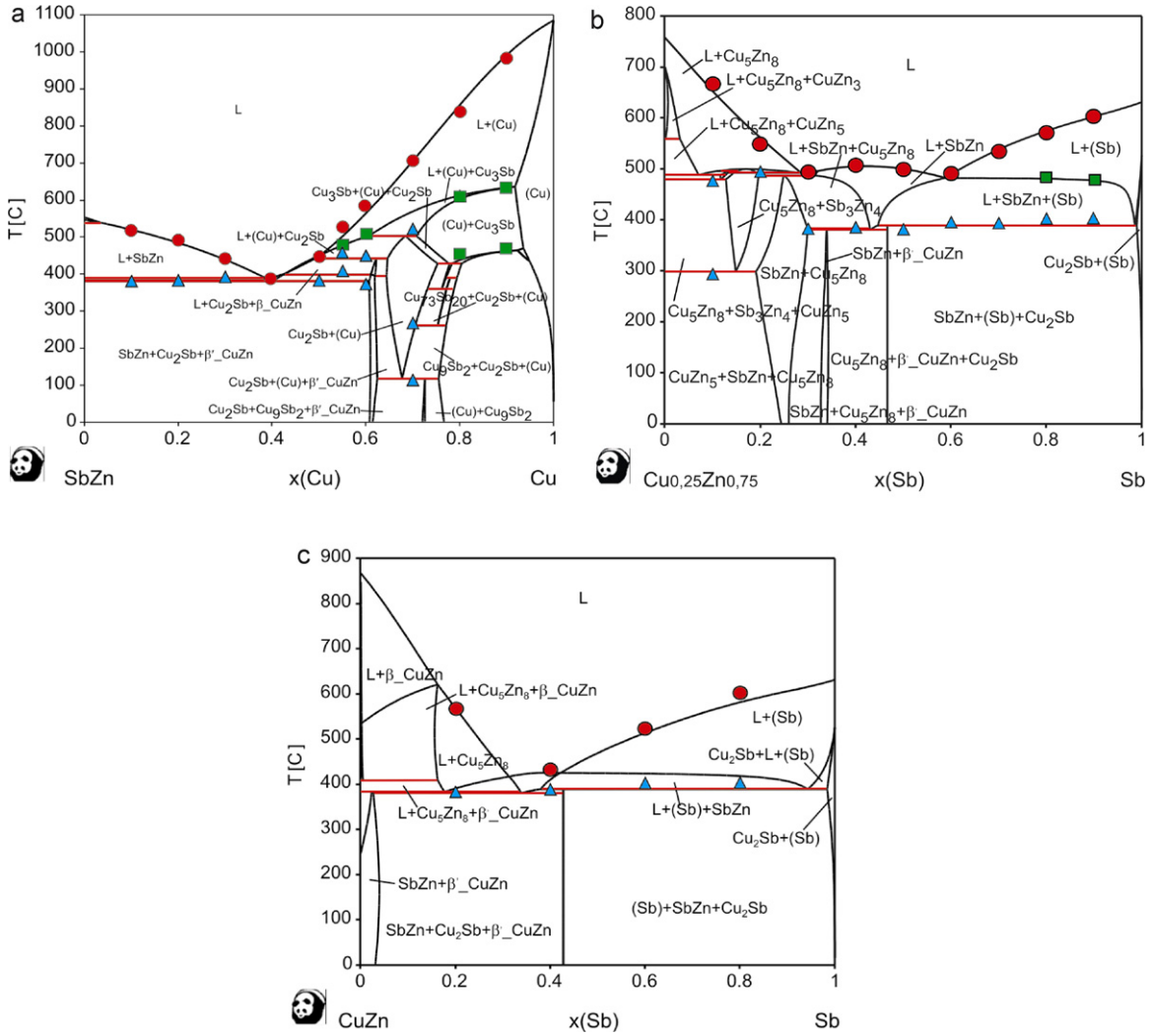

Fig. 4. Calculated vertical sections of the Cu–Sb–Zn ternary system: (a) Sb:Zn = 1, (b) Cu:Zn = 1:3 and (c) Cu:Zn = 1 compared with DSC results from the present study.

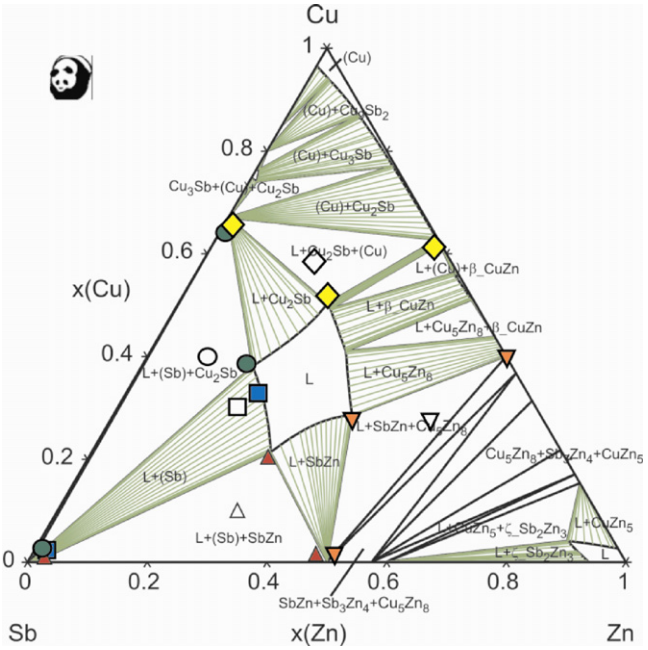

Fig. 5. Isothermal section of the ternary Cu–Sb–Zn system at 450 °C with marked experimentally determined phase compositions of the samples: 1(△), 2(□), 3(○), 4(▽) and 5(◊).

where the interaction parameters, describing the mutual interaction among constituents i and j, are denoted as ${}^{Z}L$. The liquid phase and solid solution phases are modeled this way, but more complex phases, such as intermetallic compounds, are usually modeled using the compound energy formalism [7]. Additional terms that are necessary for the proper description of the Gibbs energy from Eq. (1) are G^{ϕ}_{mag} which is the magnetic contribution and the pressure term G^{ϕ}_{P}.

In the present study, for the thermodynamic functions of the pure elements in their stable and metastable states, the phase stability equations compiled by Dinsdale [1] were used.

The phases from constitutive binary subsystems considered for thermodynamic binary-based prediction with their Pearson's symbols are listed in Table 1.

4. Literature data

4.1. Binary systems

Generally speaking, properties of the constitutive Cu–Sb, Sb–Zn and Cu–Zn binary systems were previously investigated by a number of authors [9–21]. Optimized thermodynamic parameters for the analyzed constitutive binary systems which were used in this study are therefore taken from the literature. For the binary Cu–Sb and Sb–Zn systems the thermodynamic data were taken from Liu et al. [9] and for the binary Cu–Zn system from Kowalski and Spencer [10].

The calculated phase diagrams of Cu–Sb, Cu–Zn and Sb–Zn constitutive binary systems are presented in Fig. 1.

The calculated results (Fig. 1) show good overall agreement with the experimental data taken from the literature [22,23,19]. The observed discrepancies between experimentally determined and calculated binary diagrams can be attributed to the fact that in the calculation process the compounds were considered as stoichiometric.

Given that the data for Cu–Sb system were taken from the assessment presented by Liu et al. [9] it should be noted that this assessment represents a significant improvement compared to previous studies [24,25] as β phase has been treated as disordered bcc phase (BCC_A2). However, further modeling of γ phase (CUSB_GAMMA) [9], by using model for the HCP_A3 phase, will be necessary, with consideration to the real crystallographic structure over the range of homogeneity.

The estimated data for Cu–Zn system taken from the study of Kowalski and Spencer [10] show good agreement with the experimentally obtained data for this system. The used data set includes data for both: ordered B2_BCC phase and associated disordered BCC_A2 phase. According to the results presented in [26] δ phase ($CuZn_3$) is modeled as BCC_A2, while the ordering temperature of the structure BCC_A2 → B2_BCC is concentration dependent within the range 454–467 °C.

The data for Sb–Zn system, taken from Liu et al. [9] as well, showed a good agreement between calculated and experimental values.

4.2. Cu–Sb–Zn ternary system

One of the earliest studies of the alloys of ternary Cu–Sb–Sn system by Keese [27] included investigation of the influence of antimony on the mechanical properties, Brinell hardness measurements and the isothermal section at 25 °C. In a more contemporary study Peng et al. [24] determined activities of Zn at 973 K in alloys of ternary Cu–Sb–Zn system by using EMF method and calculated thermodynamic values based on those results. These values are compared to the thermodynamic values obtained using four different models: Kohler, Colinet, Hillert and Toop. The experimentally obtained values showed a good agreement with the calculated ones obtained using Hillert and Toop's model.

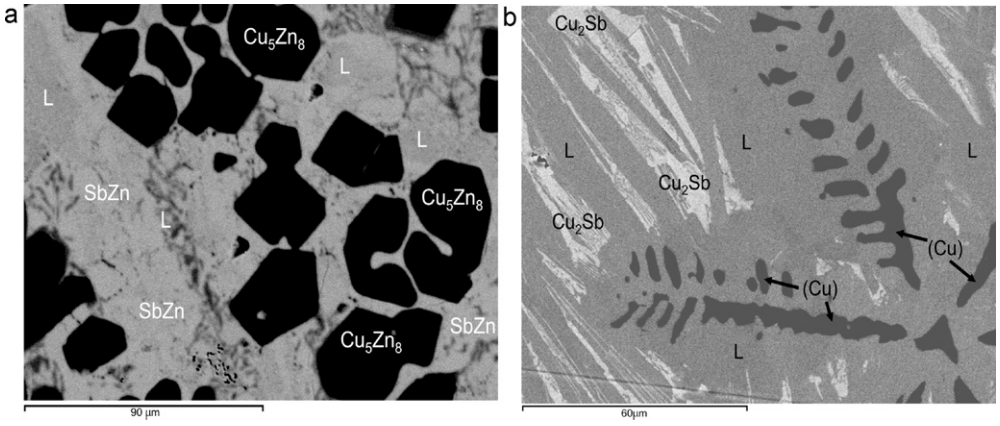

Fig. 6. SEM micrographs of the microstructures of the samples: (a) 4 and (b) 5.

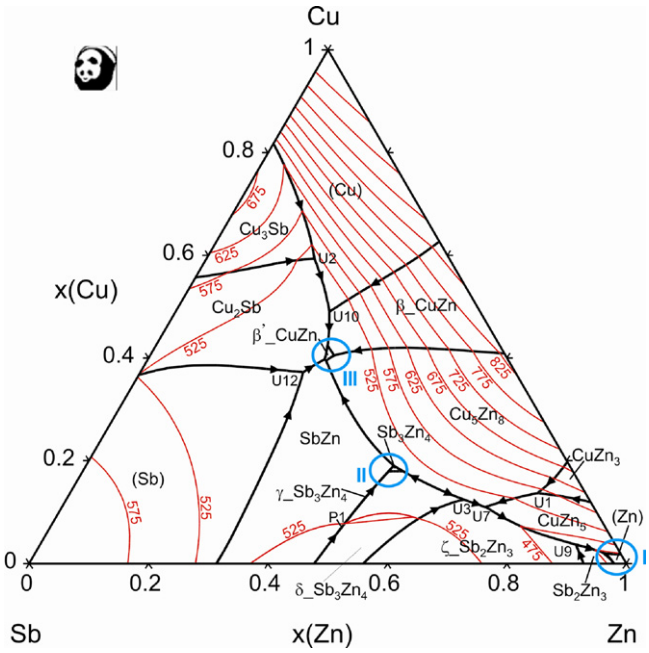

Fig. 7. Calculated liquidus projection of the ternary Cu–Sb–Zn system.

Experimentally obtained values of Zn activity for four vertical sections in the ternary Cu–Sb–Zn system at 973 K were determined by EMF method by Peng and Mlkula [25]. More recently, the activities of Zn for the same vertical sections were calculated using Miedema model and Tanaka equations by Jiang et al. [26].

In the current study, values of the activities of Zn for two vertical sections ($Cu_{50}Sb_{50}$–Zn and $Cu_{33.33}Sb_{66.67}$–Zn) were calculated. The predicted values show good agreement with the experimental results from the literature [25,26]. Comparative presentation of the calculated and the literature values of the activities of Zn for the selected vertical sections of the ternary Cu–Sb–Zn system is given in Fig. 2.

5. Results and discussion

Experimentally determined liquidus temperatures for three vertical sections: Cu:Zn = 1:3, Cu:Zn = 1 and Sb:Zn = 1 as well as temperatures of invariant and monovariant reactions, determined by DSC method, are given in Table 2.

The obtained DSC curves of the analyzed $Cu_{0.6}Sb_{0.2}Zn_{0.2}$ and $Cu_{0.55}Sb_{0.225}Zn_{0.225}$ alloy samples are presented in Fig. 3.

Calculated phase diagrams for three vertical sections together with experimentally determined liquidus temperatures and temperatures of invariant and monovariant reactions are presented in Fig. 4. The temperatures of invariant reactions are marked with blue triangles, liquidus temperatures are marked with red circles, while temperatures of monovariant reactions are marked with green rectangles. (For interpretation of the references to color in text, the reader is referred to the web version of this article.)

As can be seen from Fig. 4, the calculated and experimentally obtained phase transition temperatures are in good agreement.

Thermodynamic assessment of the ternary Cu–Sb–Zn system included calculation of the isothermal section at 450 °C as well. In order to provide better insight into the microstructure of the alloys and validate the results of calculation, five samples were investigated using SEM-EDS method. The existing phases in the

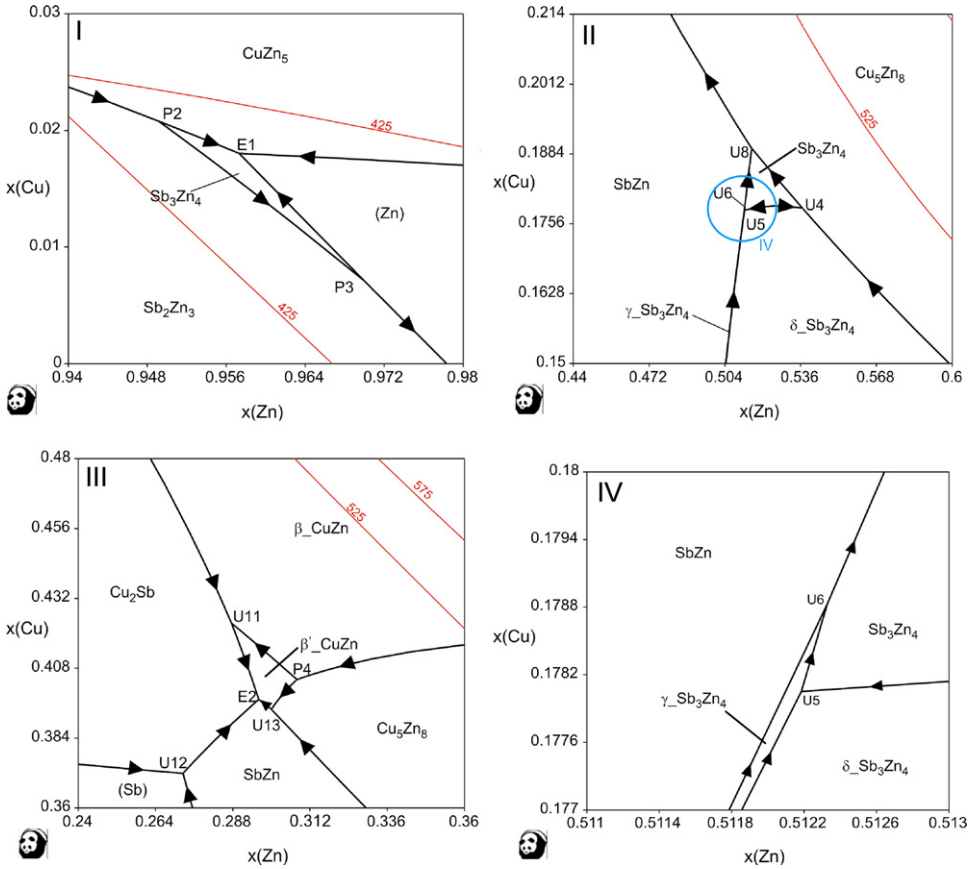

Fig. 8. Enlarged details of the liquidus projections of the Cu–Sb–Zn ternary system in a vicinity of: (I) P2, P3 and E1 points; (II) U4, U5, U6 and U8 points; (III) E2, U11, U12, U13 and P4 points; (IV) U5 and U6 points.

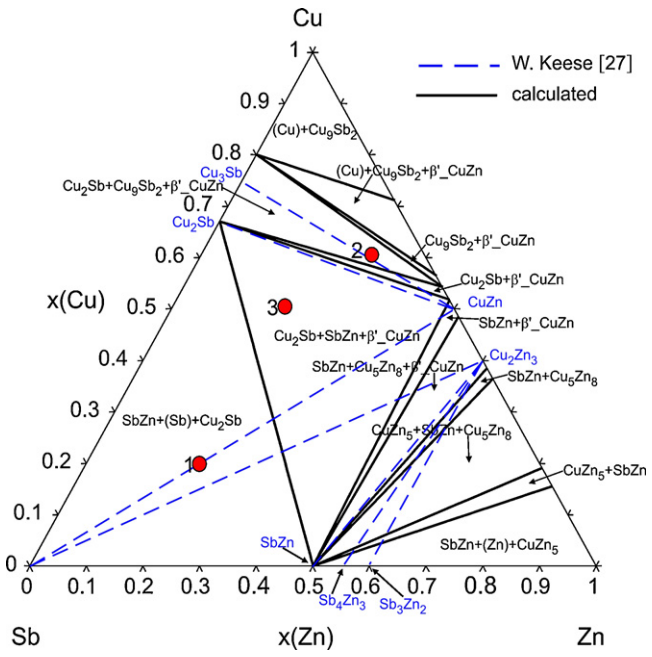

Fig. 9. Comparative presentation of calculated and experimentally determined isothermal sections of the ternary Cu–Sb–Zn system at 25 °C.

microstructure of the investigated samples are defined by the EDS point analysis of chemical composition. The overall compositions of samples and experimentally determined compositions of the coexisting phases as well as the calculated phase compositions are given in Table 3.

The calculated isothermal section of the ternary Cu–Sb–Zn system at 450 °C and experimentally determined phase compositions for samples 1(△), 2(□), 3(○), 4(▽) and 5(◊) are presented in Fig. 5. The experimentally determined compositions of present phases are marked with color filled marks. All phases in one alloy sample are marked by the same mark and the same color. (For interpretation of the references to color in text, the reader is referred to the web version of this article.)

In the calculated isothermal section (Fig. 5) there are 32 regions present, two of them represent liquid phase, one is single phase region (Sb), 12 are two-phase regions and 17 of them are three-phase regions. Four out of the five analyzed alloy samples are from three phase region (L+(Sb)+SbZn, L+(Sb)+Cu_2Sb, L+(Cu)+Cu_2Sb and L+SbZn+Cu_5Zn_8) and the fifth sample is from two-phase region (L+(Sb)). A good agreement of calculated and experimental results can be seen in Fig. 5.

SEM images of the microstructures of the two analyzed samples (4 (▽) and 5 (◊)) are presented in Fig. 6.

Experimentally determined phase compositions (Fig. 6) of considered alloys confirm existence of the calculated three-phase regions (Fig. 5).

Based on the values of the thermodynamic parameters included in COST 531 database the liquidus projection of the Cu–Sb–Zn ternary system is calculated and plotted in Fig. 7.

In the calculated liquidus projection there are 13 larger regions of primary crystallization ((Cu), Cu_3Sb, Cu_5Zn_8, β_CuZn, $CuZn_5$, $CuZn_3$, (Zn), Sb_2Zn_3, ζ_Sb_2Zn_3, δ_Sb_3Zn_4, SbZn, (Sb) and Cu_2Sb) and four smaller regions. Given that some regions of primary crystallization are very small, or hardly visible on the liquidus projection graph plotted in Fig. 7, the enlarged details of the liquidus projection in a vicinity of certain invariant points are presented in Fig. 8.

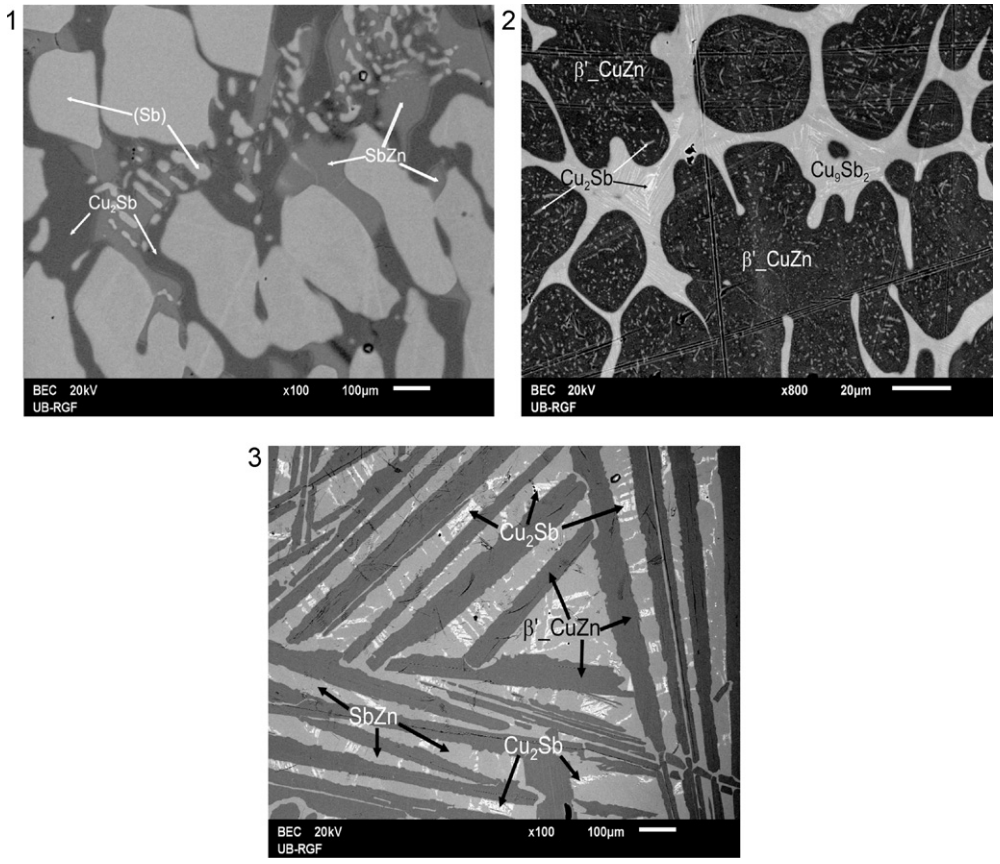

Fig. 10. SEM micrographs of the alloy samples: (1), (2) and (3).

Table 4
Predicted invariant reactions in the Cu–Sb–Zn ternary system.

Type	T (°C)	Reactions	Composition (at.%)		
			Cu	Sb	Zn
U1	558.74	$CuZn_3 \rightarrow L + Cu_5Zn_8 + CuZn_5$	13.57	8.22	78.21
P1	527.86	$L + \delta\_Sb_3Zn_4 + SbZn \rightarrow \gamma\_Sb_3Zn_4$	7.26	43.88	48.86
U2	502.28	$L + Cu_3Sb \rightarrow Cu_2Sb + (Cu)$	59.25	22.64	18.11
U3	494.84	$L + \delta\_Sb_3Zn_4 \rightarrow Cu_5Zn_8 + \xi\_Sb_2Zn_3$	12.33	21.06	66.61
U4	491.76	$L + \delta\_Sb_3Zn_4 + Cu_5Zn_8 \rightarrow Sb_3Zn_4$	17.84	28.48	53.68
U5	491.75	$L + \gamma\_Sb_3Zn_4 + \delta\_Sb_3Zn_4 \rightarrow Sb_3Zn_4$	17.8	30.97	51.23
U6	491.41	$L + \gamma\_Sb_3Zn_4 \rightarrow SbZn + Sb_3Zn_4$	17.88	30.88	51.24
U7	487.56	$L + Cu_5Zn_8 \rightarrow \xi\_Sb_2Zn_3 + CuZn_5$	10.93	18.1	70.97
U8	486.56	$L + Sb_3Zn_4 \rightarrow Cu_5Zn_8 + SbZn$	18.93	29.53	51.54
U9	444.27	$L + \xi\_Sb_2Zn_3 \rightarrow CuZn_5 + Sb_2Zn_3$	3.6	6.68	89.72
U10	441.19	$L + (Cu) \rightarrow Cu_2Sb + \beta\_CuZn$	48.95	25.29	25.76
P2	416.81	$CuZn_5 + Sb_2Zn_3 \rightarrow L + Sb_3Zn_4$	2.07	3.01	94.92
P3	409.82	$L + Sb_3Zn_4 \rightarrow Sb_2Zn_3 + (Zn)$	0.71	2.29	97
E1	409.71	$L \rightarrow Sb_3Zn_4 + (Zn) + CuZn_5$	1.8	2.47	95.73
P4	408.29	$\beta\_CuZn + Cu_5Zn_8 \rightarrow L + \beta'\_CuZn$	40.4	28.8	30.8
U11	397.7	$L + \beta\_CuZn \rightarrow Cu_2Sb + \beta'\_CuZn$	42.34	28.9	28.76
U12	388.37	$L + (Sb) \rightarrow SbZn + Cu_2Sb$	37.17	35.57	27.26
U13	382.54	$L + Cu_5Zn_8 \rightarrow \beta'\_CuZn + SbZn$	39.38	30.62	30
E2	380.01	$L \rightarrow SbZn + Cu_2Sb + \beta'\_CuZn$	39.71	30.68	29.61

The predicted invariant reactions in ternary Cu–Sb–Zn system are listed in Table 4, together with the reaction temperatures, corresponding types of those invariant reactions and the compositions at which the reactions occurred.

Altogether, there are 19 reactions. Two of them are E-type reactions ($L \rightarrow \alpha + \beta + \gamma$) and those are ternary eutectic reactions. Thirteen of them are U-type reactions and 10 of them are transition reactions ($L + \alpha \rightarrow \beta + \gamma$). Four reactions are P-type, and those are peritectic reactions ($L + \alpha + \beta \rightarrow \gamma$) i.e. formation reactions.

The ternary Cu–Sb–Zn system was further thermodynamically assessed by calculation of the isothermal section at 25 °C. Comparative presentation of the calculated and experimentally determined (Keese [27]) isothermal sections is presented in Fig. 9.

The isothermal section determined by Keese [27] is divided into eight triangles: Cu_3Sb–CuZn–Cu, Cu_3Sb–CuZn–Cu_2Sb, Cu_2Sb–CuZn–Sb, CuZn–Sb–Cu_2Zn_3, Sb–Cu_2Zn_3–ZnSb, ZnSb–Cu_2Zn_3–Zn_4Sb_3, Zn_4Sb_3–Cu_2Zn_3–Zn_3Sb_2 and Cu_2Zn_3–Zn_3Sb_2–Zn. These eight regions are marked by dashed lines in Fig. 9. However, in the calculated isothermal section there are 13 regions, seven of them are three-phase regions and six of them are two-phase regions.

In order to gain more information about the microstructure and composition of the alloys from the calculated three-phase regions (Fig. 9), especially considering the observed discrepancy between the presented sections, three alloy samples were investigated using SEM-EDS method. The samples with the following compositions were analyzed: sample 1 (x(Sb) = 0.6; x(Zn) = 0.2; x(Cu) = 0.2), sample 2 (x(Sb) = 0.1; x(Zn) = 0.3; x(Cu) = 0.6) and sample 3 (x(Sb) = 0.3; 20 x(Zn) = 0.2; x(Cu) = 0.5). The obtained microstructures are presented in Fig. 10.

From Fig. 10 it is evident that experimentally defined phases, present in the microstructures of the considered alloys, are in a good agreement with theoretically predicted phase regions. Contrary to the published study [27], the results of EDS analysis confirm the presence of three phases in all three samples, sample 1 (Cu_2Sb + SbZn + (Sb)), sample 2 (Cu_2Sb + Cu_9Sb_2 + β'_CuZn) and sample 3 (Cu_2Sb + SbZn + β'_CuZn), thus corroborating presence of the three-phase regions in the calculated isothermal section (Fig. 9).

6. Conclusion

Phase diagram of the Cu–Sb–Zn ternary system has been investigated experimentally by DSC and SEM-EDS techniques and theoretically by CALPHAD method. Calculated constitutive binaries and predicted activities of Zn for two vertical sections of the investigated ternary system were found to be in a good agreement with the experimental results from the literature. Melting behavior of the different Cu–Sb–Zn alloys has been determined and the invariant reactions and the types of reactions were defined. The calculated liquidus temperatures show reasonable agreement with the DSC results from the present study. The isothermal section at 450 °C has been calculated and validated by SEM-EDS analysis. Additionally, the isothermal section at 25 °C has been calculated as well and compared with the results from the literature. Contrary to the literature data, the results of SEM-EDS analysis confirm presence of three phases in investigated samples, thus corroborating existence of the three-phase regions in the calculated isothermal section.

Acknowledgements

This work was supported by Ministry of Science of the Republic of Serbia under Project ON 172037. Calculations were performed by Pandat 8.1 software.

References

[1] A.T. Dinsdale, SGTE Unary Database, Version 4.4, 2002, www.sgte.org.
[2] A.T. Dinsdale, A. Kroupa, J. Vízdal, J. Vrestal, A. Watson, A. Zemanova, COST Action MP0602, Version 1.0, Thermodynamic Database, Brno, Czech Republic, 2009.
[3] N. Saunders, A.P. Miodownik, CALPHAD (A Comprehensive Guide), Elsevier, London, 1998.
[4] H.L. Lukas, S.G. Fries, B. Sundman, Computational Thermodynamics: CALPHAD Method, Cambridge University Press, Cambridge, UK, 2007.
[5] O. Redlich, A. Kister, Ind. Eng. Chem. 40 (1948) 345.
[6] Y.-M. Muggianu, M. Gambino, J.-P. Bros, J. Chem. Phys. 72 (1975) 83.
[7] J.-O. Andersson, A. Fernandez-Guillermet, M. Hillert, B. Jansson, B. Sundman, Acta Metall. 34 (1986) 437.
[8] A.T. Dinsdale, A. Kroupa, J. Vizdal, J. Vrestal, A. Watson, A. Zemanova, COST Action 531—Atlas of Lead Free Soldering, vol. 1, COST Office, Brussels, Belgium, 2008.
[9] X.J. Liu, C.P. Wang, I. Ohnuma, R. Kainuma, K. Ishida, J. Phase Equilib. 21 (5) (2000) 432–442.
[10] M. Kowalski, J.P. Spencer, J. Phase Equilib. 14 (4) (1993) 432–440.
[11] D. Živković, D. Minić, D. Manasijević, A. Kostov, N. Talijan, L. Balanović, A. Mitovski, Ž. Živković, JMM Sect. B: Metall. 46 (1) (2010) 105–111.
[12] D. Manasijević, D. Minić, D. Živković, J. Vřešťál, A. Aljilji, N. Talijan, J. Stajić-Trošić, R. Todorović, CALPHAD 33 (1) (2009) 221–226.
[13] D. Jendrzejczyk-Handzlik, M. Rechchach, W. Gierlotka, H. Ipser, H. Flandorfer, Thermochim. Acta 512 (1–2) (2011) 217–224.
[14] T.B. Massalski, Binary Alloy Phase Diagrams, vol. 2, 2nd edition, The Materials Information Society, Materials Park, OH, 1990.
[15] E. Günzel, K. Schubert, Z. Metallkd. 49 (1958) 124–131.
[16] T. Murakami, N. Shibata, Sci. Rep. Tohoku Imp. Univ. 25 (1936) 527–568.

[17] V. Izard, M.C. Record, J.C. Tedenac, S.G. Fries, CALPHAD 25 (2001) 567–581.
[18] X.J. Liu, C.P. Wang, I. Ohnuma, R. Kainuma, K. Ishida, J. Phase Equilib. 21 (2000) 432–442.
[19] M. Hansen, K. Anderko, Constitution of Binary Alloys, McGraw-Hill Book Comp., New York, 1958.
[20] G.V. Raynor, Annoted Equilibrium Diagrams, Series No. 3, The Institute of Metals, London, 1944.
[21] R. Nitsche, S.A. Mey, K. Hack, P. Spencer, Z. Metallkd. 82 (1991) 67–72.
[22] W. Gierlotka, D. Jendrzejczyk-Handzlik, J. Alloys Compd. 484 (2009) 172–176.
[23] J.-B. Li, M.-C. Record, J.-C. Tedenac, J. Alloys Compd. 438 (2007) 171–177.
[24] M. Peng, Z. Qiao, A. Mlkula, CALPHAD 20 (1) (1996) 69–78.
[25] M. Peng, A. Mlkula, Z. Metallkd. 86 (4) (1995) 228–233.
[26] G. Jiang, Y. Liu, Y. Li, Y. Su, J. Guo, Acta Metal. Sin. 43 (5) (2007) 503–508.
[27] W. Keese, Z. Metallkd. 28 (3) (1936) 58–63.